Title: Stochastic and coincident control of terminal cell differentiation and cell cycle exit

Authors: Michael L. Zhao[1], Kyle M. Kovary[1], Atefeh Rabiee[1], Zahra Bahrami-Nejad[1], Brooks Taylor[1], and Mary N. Teruel[1,*]

Affiliations:
[1]Dept. of Chemical and Systems Biology, Stanford University, Stanford, CA

***Corresponding Author:** mteruel@stanford.edu

SUMMARY

Terminal cell differentiation is essential for developing and maintaining tissues in all multi-cellular organisms. However, the relationship and timing between irreversible cell-cycle exit and irreversible differentiation is not well understood. Using adipogenesis as a model system for terminal cell differentiation, we delineate the timing between cell cycle exit and terminal differentiation by live-cell imaging of cell cycle reporters and expression of PPARG, a master regulator of differentiation. During terminal differentiation, the levels of PPARG and of the CDK inhibitor p21 are coupled after mitosis, and both gradually increase. The increase in p21 expression generates a variable, extended G1 phase that allows some cells to reach the PPARG threshold for differentiation before cells enter the next cell cycle and PPARG is again suppressed. Thus, by way of extending the duration of G1 phase during terminal differentiation, precursor cells can stochastically control the number of cell divisions and the total number of differentiated cells.

HIGHLIGHTS

- Development of an experimental model system to study the timing between terminal cell differentiation and cell-cycle exit
- Depending on the levels of PPARG and CDK inhibitors (e.g. p21) during an extended G1 after mitosis, cells stochastically commit to either differentiate or enter another round of cell division
- Cells permanently exit the cell cycle in G1 by further increasing CDK inhibitors after they increase PPARG beyond a threshold for differentiation
- Cells control the number of terminally differentiated cells by regulating PPARG versus CDK inhibitor expression and thereby regulate the number of cell divisions before differentiation.

INTRODUCTION

Terminal differentiation typically requires the transition of proliferative precursor cells into post-mitotic differentiated cells characterized by prolonged or permanent withdrawal from the cell cycle. In metazoans, disruption of this critical transition affects the balance between the number of differentiated and precursor cells and loss of this control can lead to the disruption of tissue homeostasis, development of cancer, and metabolic disorders (Biteau et al., 2011; Ghaben and Scherer, 2019; Hanahan and Weinberg, 2011; Ruijtenberg and van den Heuvel, 2016). An important early finding supporting a molecular link between differentiation and cell cycle arrest showed that the muscle specific transcription factor, MyoD, was sufficient to upregulate the cyclin dependent kinase inhibitor, p21, to inhibit cell cycle activity in a p53-independent manner (Guo et al., 1995; Halevy et al., 1995). Indeed, the link between p21 expression and terminal differentiation seemed to be widespread across different terminally differentiated cells (Parker et al., 2006). It was also observed that lineage specific transcription factors, such as CEBPA, possess anti-mitotic activity independently of its transcriptional activity possibly by inhibiting cyclin-CDKs (Harris et al., 2001; Umek et al., 1991). More recent work has added additional components to the regulation of cell cycle exit during terminal differentiation, for example, by demonstrating a role for other CDK inhibitors, suggesting parallel inhibitory pathways, and identifying redundancy among cell cycle exit regulators in a tissue specific manner (Buttitta et al., 2007; Ruijtenberg et al., 2015; Zalc et al., 2014). Taken together, these prior studies establish a rich set of molecular connections between the regulators of terminal differentiation and the control of cell cycle exit.

However, in terminal cell differentiation processes such as skin renewal, adipose tissue expansion, and development of the Drosophila eye, quiescent precursor cells have been reported to go through one of more rounds of division as part of the proliferation-differentiation transition (Aragona et al., 2017; Baonza and Freeman, 2005; Jeffery et al., 2015). Regulation of CDK activity clearly plays a critical role as mice lacking the CDK inhibitors p21, p27, or both have synergistically up to 6 times higher fat mass (Naaz et al., 2004). These observations raise the following questions: when along the differentiation trajectory is the post-mitotic state established and how do cells

coordinate cell cycle exit with the expression of regulators of terminal differentiation during this highly dynamic transition period? Even in *C. elegans*, where cell lineages are highly stereotyped, it is not well understood how developmental factors coordinate with the canonical cell cycle regulators to regulate differentiation (Kipreos and van den Heuvel, 2019). Since cell division and differentiation are often asynchronous processes with different timescales, it has been difficult to precisely define the order of events during the proliferation-differentiation decision and the relationship between cell division and differentiation. Interestingly, some terminal differentiation processes have been reported to have a precise number of cell divisions before differentiation (Hsu et al., 2014; Insco et al., 2009), while others suggested more variable numbers of divisions (Clayton et al., 2007; Jones et al., 2007), raising the question what may cause this apparently stochastic behavior. A major challenge to address some of these fundamental questions has been the inability to dynamically monitor differentiation and cell cycle progression simultaneously in the same cell (Ruijtenberg and van den Heuvel, 2016).

Furthermore, a key parameter that has been missing and that is essential to be able to understand the relationship between the cell cycle and terminal cell differentiation is a marker that defines the precise time when a cell irreversibly commits to the differentiated state. Many terminal cell differentiation systems including adipogenesis and myogenesis are regulated by a cascade of transcription factors (Blais et al., 2005; Farmer, 2006). What is essential to establish a temporal marker for commitment in any differentiation system is to determine which of the factors in the transcriptional cascade exhibits bimodal behavior and can thus be used to demarcate undifferentiated from differentiated cells. For example, even though the early transcription factor CEBPB is required for adipogenesis, it is not a suitable marker of commitment. CEBPB levels increase in all cells that are subjected to the DMI adipogenic stimulus, but the levels are not predictive of whether or not a cell while continue on to differentiate once the stimulus is removed (Bahrami-Nejad et al., 2018). However, in previous work using single-cell imaging, we showed that the transcription factor PPARG is a suitable marker for commitment in adipogenesis because it exhibits bimodal behavior, and a threshold level of PPARG can be used to distinguish

undifferentiated from differentiated cells (Figure 1A) (Ahrends et al., 2014; Park et al., 2012). We also went on to show that such a PPARG threshold mechanism allows the fraction of precursor cells that undergo adipocyte differentiation to be controlled by pulsatile hormonal stimuli patterns (Bahrami-Nejad et al., 2018). This current study more clearly defines this concept of a PPARG threshold and demonstrates that PPARG levels can be used to mark a precise time when cells irreversibly commit to differentiate. If the level of PPARG in a cell has not reached the threshold level, the cell will revert back to an undifferentiated state when the differentiation stimulus is removed. In contrast, once the PPARG level in the cell has reached the threshold value, the positive feedbacks to PPARG will be so strong that the cell will keep increasing its PPARG level even if the differentiation stimulus is removed and will thus continue onto reach the fully differentiated adipocyte state (Bahrami-Nejad et al., 2018). We use here the term “commitment” to describe this PPARG threshold which is a precise timepoint that marks an irreversible point-of-no return for a cell to differentiate.

Here we established a method to track both the expression of PPARG and cell cycle progression in living cells by combining the widely used FUCCI sensor with our fluorescent PPARG sensor for adipocyte differentiation (Bahrami-Nejad et al., 2018; Sakaue-Sawano et al., 2008). Our live-cell experiments temporally and mechanistically link the commitment point for terminal differentiation to the last mitotic exit as cells undergo a terminal cell cycle arrest. We show that the link between terminal mitotic exit and the irreversible commitment point for differentiation is controlled by the expression of the CDK inhibitor p21 and that the PPARG threshold marks the point when p21 reaches sufficient levels to make cells unresponsive to serum stimulation. Markedly, we show how a dynamic differentiation network coordinates the expression of CDK inhibitors in mothers and early daughters to bring cells into a terminally-arrested state, further highlighting the importance of live cell analysis in establishing the ordering of events during the transition from proliferative precursors to post mitotic differentiated cells.

RESULTS

Measurement of the precise time when cells irreversibly commit to differentiate based on live single-cell analysis of the expression level of PPARG

A major bottleneck in trying to understand the relationship between exit from the cell cycle and irreversible commitment to the differentiated state is the lack of a quantitative live-cell readout for when differentiation commitment has occurred (Buttitta and Edgar, 2007). Thus, we first established this critical live-cell readout that can dynamically mark the point in time when an individual cell irreversibly commits to the terminally differentiated state. In previous work, we had shown with immunocytochemistry that a commitment point occurs in adipogenesis and is regulated by a bi-stable switch mechanism (Park et al., 2012). We also showed that fluorescently tagged endogenous PPARG, the master transcriptional regulator of adipogenesis, can be used as a live-cell reporter for differentiation state (Bahrami-Nejad et al., 2018)(Figures 1A and 1B). To precisely determine when a PPARG threshold is reached, we compared the PPARG levels at the 48-hour timepoint when the stimulus was removed versus PPARG levels at the 96-hour timepoint, 2 days after the stimulus was removed (Figure 1C). This analysis demonstrated that a precise PPARG threshold level indeed exists, such that cells with PPARG levels higher than the critical threshold went on to differentiate while the majority of cells below the threshold remained undifferentiated. As different microscope parameters and cell culture conditions can change between experiments, it should be noted that the PPARG threshold value is calculated in each experiment from an analysis of the level of PPARG at the time of adipogenic (DMI) stimulus removal that determines differentiation outcome (see Methods section). Critically, we also confirmed that citrine-PPARG fluorescence correlates with many commonly used markers of adipogenesis (Figure 1D).

To better define the properties of this citrine-PPARG commitment point, we estimated its predictability by asking how well a given level of PPARG at 24, 48 and 72 hours can predict the differentiation fate outcome at 96 hours, 48 hours after removal of the hormone stimuli (Figure 1E). We estimated the differentiation probability at the three time points by binning cells into groups according to their PPARG levels. For each PPARG intensity bin, we plotted the fraction of cells that

were above the PPARG threshold at the end of the experiment. The data takes the shape of a logistics curve and shows that PPARG levels were highly predictive of final differentiation fate at all three timepoints. As a comparison, both the integral and derivative values of PPARG served as poorer predictors of the final differentiated state (Figure S1). Furthermore, the curves are closely spaced, and the value used to estimate the PPARG threshold point corresponded to a greater than 70% differentiation probability for all three time points (Figure 1E). Interestingly, the probability of differentiation in cells at the start of the experiment did not exhibit a strong dependence on PPARG, suggesting that the PPARG threshold represents a decision point that is generated in response to addition of a differentiation stimulus and is not just simply a predetermined feature of the cells.

Next, we investigated whether the PPARG threshold marks a qualitative change in PPARG dynamics as would be expected in a bistable system. We computationally aligned single cell traces by the time in which the cell crossed the threshold. This analysis shows that the threshold indeed marks a point where PPARG dynamics change from being stably low to stably high (Figure 1F). Analysis of the PPARG derivative around this threshold point also showed that the change occurred fast relative to the four-day time course, with a large increase in PPARG occurring in a 3-hour window around the threshold point (Figure S2). Lastly, we found that PPARG only began to positively correlate with endpoint measurements of adipocyte markers after the PPARG threshold is reached (Figure 1G). Our analysis shows that the PPARG threshold represents the point where precursor cells begin to become mature fat cells and therefore defines a differentiation commitment point in single cells.

Development of a system to measure terminal differentiation and cell division at the single-cell level

In the same cells expressing the endogenous citrine-PPARG shown in Figure 1, we had also transfected in a cell cycle reporter in order to be able to study the dynamic transition from proliferative precursors to post mitotic terminally differentiated cells (Figure 2A). This cell cycle reporter is half of the FUCCI sensor pair and is composed of a fragment of the geminin protein fused

to the red fluorescent protein, mCherry (Sakaue-Sawano et al., 2008). The sensor is expressed under the control of a constitutively active promoter, and the fluorescent signal is nuclear-localized and dependent on the activity of the anaphase promoting complex/cyclosome (APC/C) (Cappell et al., 2016). When APC/C activity is turned off near the G1-to-S phase transition, the geminin protein sensor begins to accumulate to high levels. When APC/C activity is turned on in anaphase during mitosis, the sensor is rapidly degraded, and fluorescence returns to near background levels. The cells were also stably transfected with fluorescently-labeled H2B in order to enable automated nuclear tracking.

We performed differentiation experiments under subconfluent conditions such that the majority of cells could undergo one or more divisions without contacting other cells. These conditions yielded 20-50% differentiated cells after 4 days of differentiation compared to ~80% differentiation rate under more confluent conditions (Figure S3). We chose these conditions to maximize the number of cell divisions, reduce the effect of cell density on cell cycle arrest, and improve fidelity of the automated tracking algorithm by reducing cell crossover events. To determine the timing between cell cycle phase and differentiation commitment, we carried out live-cell imaging experiments on our dual reporter cells while inducing differentiation by application of an adipogenic stimulus. By imaging mCitrine fluorescence over the course of differentiation and tracking thousands of cells, we are able to visualize the progression through differentiation at the single cell level and are further able to separate differentiating from undifferentiated cells (Figure 2B). Furthermore, our live cell system allows quantitative measurements of parameters such as the number of division events, differentiation state, and the length of cell cycle phases, all in the same cell (Figure 2C-2E). As shown in the histogram in Figure 2C and single-cell traces in Figure 2E, there is great variability in the number of mitosis cells undergo before differentiating. Also, there is great variability in the time after stimulation that cells start to increase PPARG levels and in how long after the last mitosis cells reach the PPARG threshold.

Cells preferentially commit to differentiate out of an extended G1-phase.

The single-cell timecourses in Figure 2E showed that there is a clear correlation that a PPARG increase to the threshold is only observed after the end of the last mitosis. This point can also be shown by differentiating and analyzing cells stably transfected with a CDK2 reporter (Spencer et al., 2013). CDK2 activity starts to increase at the start of G1 phase and gradually increases until mitosis when it drops back to basal levels at anaphase before the two daughter cells are born. Markedly, the same time-course analysis shows that the PPARG threshold is reached almost exclusively in G1, when both geminin and CDK2 activity are low (example shown in Figure 3A, left). The generality of this observation is confirmed by a scatter plot analysis of hundreds of cells at all time points during differentiation which shows that PPARG levels are high only when CDK2 activity levels are low (Figure 3A, right).

Most cells committed to differentiate only after the last mitosis was completed, with an average delay of approximately 14 hours (Figure 3B). By analyzing cells that underwent multiple divisions before differentiating, we found that the time it takes to reach the PPARG threshold is significantly longer than the time it takes to commit to the next cell cycle (Figure 3C). From this observation, we used the natural variation that existed in our data to ask whether the increased duration of G1 is beneficial for differentiation. We used the timecourse data shown in Figures 2B-E and binned cells into groups based on when a cell completed its last mitosis in increments of 4 hours (Figure 3D, top). In Figure 3D (bottom), we plotted two properties of the bins: 1) the fraction of cells that differentiated at Day 4 in that bin (y-axis, % PPARG high cells) and 2) the average time the cells in that bin spent in G1 before reaching the differentiation threshold (x-axis) This analysis showed a strong positive correlation between the ability of cells to differentiate and the time they spent in G1 duration before differentiation commitment, suggesting that a longer G1-phase creates a window that promotes differentiation. We ruled out that this effect was simply mediated by dilution of PPARG due to extra cell divisions (Figure S2). The length of G1 increases in cells that undergo multiple divisions before they differentiate (Figure 3E, top). During differentiation, there is a true lengthening of the G1-phase since the peaks remain similar. In the low PPARG cells that do not differentiate within the timeframe of the experiment, the G1-phase is also lengthened but the shape is very

different suggesting the cells are entering quiescence (Figure 3E, bottom). Together, our data shows that differentiation commitment largely occurs out of an extended G1-state that has to optimally lasts longer than 14 hours after mitosis.

The CDK inhibitor p21 and cyclin D, which both regulate the length of G1 phase, antagonistically regulate the number of differentiating cells.

To confirm our observation that G1 length and differentiation are correlated, we explored the role of p21 which is known to control the length of G1-phase. We found that, as expected, knockdown of p21 increased the length of G1-phase as well as overall cell cycle activity (Figure 4A, left and middle). This increase was associated by a decrease in the degree of differentiation over time (Figure 4A, left). Overexpression of human p21 using the DHFR system yielded the opposite effect, decreasing cell cycle activity and increasing the degree of differentiation (Figure 4B).

One of the main targets of EGF signaling is the upregulation of the D-type cyclins. Given the previously demonstrated role for the D-type cyclins in the regulation of adipogenesis, we tested the effect of reducing cyclin D expression on the proliferation-differentiation switch. We found that cyclin D1 knockdown led to an increase in differentiation and a decrease in cell cycle activity (Figure 4C). This was not observed to the same degree when cyclins D2 and D3 were not knocked down together. When we controlled for cell cycle variation by computationally gating for cells that had similar cell cycle properties, we found that cyclin D1 knockdown led to a large increase in PPARG expression (Figure 4D). Our data are in agreement with previously reported negative regulation of PPARG by cyclin D1 (Fu et al., 2005) and further demonstrate that this regulation exists even after controlling for cell cycle variation through computational gating of similarly cycling cells.

We next tested whether regulators of G1, such as growth factors, could also regulate the degree of differentiation. To decrease growth factor signaling activity, we lowered the fetal bovine serum (FBS) concentration from 10% to 2% or added a MEK inhibitor in the differentiation cocktail. Both conditions resulted in a decrease in cell cycle activity and a concomitant increase in differentiation (Figure 4E). Interestingly, when we added a large concentration of EGF back into the

2% FBS condition, the cells differentiated to the same degree as observed in the 10% FBS condition but did not re-enter the cell cycle in the same manner as observed in 10% FBS differentiation media (Figure 4E, left). This demonstrates that the effect of growth factors on differentiation can be separated from its effect on proliferation in our dual reporter cells. These experiments validate our observation that G1 length and differentiation are correlated and further show that the response to growth factors affects the decision to proliferate or differentiate. Taken together and as summarized in the diagram in Figure 4F, our experiments show that the decision to proliferate opposes the decision to differentiate and that canonical regulators of G1 duration also in parallel regulate the decision to differentiate.

PPARG controls cell cycle activity in part by upregulating p21 expression.

We next investigated how PPARG levels regulate cell cycle activity and entry into the post mitotic state during differentiation. Over the course of a typical differentiation experiment, we observed that cells with continued proliferation strongly correlated with persistently low levels of PPARG (Figure 2B). We validated this observation using RNA interference against PPARG, and we found that depletion of PPARG increased the fraction of proliferating cells throughout the entire time course of the experiment (Figure 5A). Based on our observation that differentiation commitment occurs in a state with low CDK2 activity and previous work identifying p21 as a major regulator of cells in the CDK2 low state, we hypothesized that the CDK inhibitors played a critical role in inhibiting cell division during adipogenesis in our cells. We performed RNA-sequencing over 6 days of differentiation in cells transfected with siRNA targeting PPARG or non-targeting siRNA. We identified two potential CDK inhibitors that could mediate cell cycle arrest during differentiation, p18 and p21 (Figure 5C). To validate p18 and p21, we knocked them down with siRNA under differentiation conditions and found that only p21 knockdown led to an increase in mitotic events (Figures 4A and 5C). To explore potential mechanisms by which p21 is upregulated during adipogenesis, we looked through our RNA-seq data set and found that FKBPL (WiSP39) was also upregulated throughout differentiation in a PPARG dependent manner (Figure 5D). FKBPL has

previously been shown to stabilize p21 and increase its ability to arrest cells in response to ionizing radiation (Jascur et al., 2005). To test if a similar mechanism could function during the early stages of differentiation, we carried out cycloheximide protein degradation experiments in which we measured the half-life of p21 in cells transfected with siRNA targeting FKBPL or a control. Our results showed that knockdown of FKBPL decreases p21 half-life but does affect the half-life of PPARG, suggesting that FKBPL does regulate p21 stability during terminal cell differentiation (Figure 5E). Lastly, we tested whether adding a direct activator of PPARG could also upregulate p21 expression. Indeed, the addition of rosiglitazone led to a robust increase in p21 expression in cells below and above the PPARG threshold (Figure 5F). However, cells above the PPARG threshold upregulated p21 to an even greater degree. Our experiments suggest that PPARG arrests the cell cycle in part through the regulation of p21 levels by both transcriptional and post-transcriptional mechanisms. Interestingly, PPARG increases slightly before the end of the last mitosis (Figure 5G), suggesting that there is a stochastic competition between proliferation and differentiation during G1-phase. To further test for an active competition between proliferation and differentiation, we assayed what the continued commitment to the cell cycle had on differentiation. A gradual reduction in the fraction of cells that proliferate is paralleled by a gradual increase in the cells that differentiate (Figure 5H, top). The cells that have not exited the cell cycle after 20 hours, as assessed by the fraction of cells in S/G2/M phases with high geminin degron signal, have a significant reduction in their likelihood to differentiate by the time the adipogenic stimulus is removed at 48 hours (Figure 5H, bottom). Together our results suggest that there is an active competition between proliferation and differentiation during G1-phase whereby a small increase in PPARG already before the start of G1-phase can act through upregulation of p21 to suppress re-engagement of the cell cycle and allow an extended time in G1 for PPARG levels to build to the differentiation commitment point. This scheme is depicted in Figure 5I.

PPARG regulates entry into a post-mitotic state during terminal differentiation

We next tested whether committing to differentiation could also mark the point in which cells

become post-mitotic. The typical differentiation protocol involves adding DMI for 48 hours and replacing the media with growth media and insulin for another 48 hours. We took advantage of this protocol and asked how a cell responded to the fresh growth media added at the 48-hour time point based on its PPARG level before the removal of DMI. We grouped cells together based on their PPARG levels at the timepoint right before DMI removal. We found that the group of cells that passed the PPARG threshold showed a flat geminin response to fresh growth media (Figure 6A). We confirmed that this represented reduced cell cycle activity by calculating the fraction of cells that underwent mitosis in response to fresh growth media as assessed by a split in the H2B nuclear signal (Figure 6B). Cells past the PPARG threshold had the lowest chance of responding to fresh growth media, suggesting that crossing the PPARG threshold also marks entry into the post-mitotic state.

We tested whether p21 also had a role in regulating cell exit during this phase of differentiation. After the completion of a live cell time course, we fixed the cells and stained for p21 expression. We again grouped cells according to PPARG levels and reported the average mean nuclear p21 fluorescence for each PPARG bin. We found a steady increase in p21 levels all the way through the PPARG threshold until it reached maximal levels after the PPARG threshold (Figure 6C). Next we transfected siRNA at the 48-hour time point to acutely knock down p21, CEBPA, and PPARG and found that only p21 knockdown led to a dramatic increase in cell cycle activity (Figure 6D, top). Successful knockdown was confirmed by endpoint immunostaining of CEBPA and p21 and by live imaging of citrine-PPARG (Figure S5). Using the same data set, we performed a similar analysis of PPARG levels and the response to freshly-added growth factors. Strikingly, p21 knockdown led to a complete loss of control of cell cycle exit by PPARG when compared to the non-targeting siRNA control as assessed by both geminin levels and the number of observed H2B splits (Figures 6E and 6F). Taken together, our data shows that the commitment to differentiation also marks the entry into a post-mitotic state and that this regulation critically depends on p21.

DISCUSSION

Our live cell experiments directly link proliferation history with the expression the master regulator of adipogenesis, PPARG. Importantly, our experimental system enabled us to estimate a point of differentiation commitment and this provided us with a reference in which to assess the relationship between cell cycle and progression through terminal differentiation. Our imaging data supports a dynamic three-phase model underlying a gradual transition, as opposed to a sudden and abrupt switch, between proliferation and terminal adipogenesis (Figure 7A). In the first phase of the model, proliferative precursors make cell cycle decisions largely independently of differentiation commitment. Cells in this early PPARG low-state are the most sensitive to the mitogens. Cell cycle activity during this time does not seem to greatly affect the likelihood of a cell to differentiate. The existence of an early proliferative window is compatible with models where cell division is required to maintain the precursor pool or initiate the differentiation process. This represents the early stages of differentiation during which commitment factors such as PPARG are expressed at minimal levels and precursor cells are free to proliferate. The existence of such a window is explained by our previous finding that PPARG depends on the regulation of slow commitment factors which create a delay in the rise of PPARG in response to adipogenic stimuli.

As PPARG expression begins to increase after about one day, cells enter a second phase where there is a tradeoff between the decision to divide and the decision to differentiate. Cells that continue to proliferate during this phase reduce their likelihood of differentiating by the end of the experiment. A likely source of this competition is explained by a shared set of canonical regulators of the G1 phase that regulate, in parallel, the decision to cycle and the decision to differentiate. Surprisingly we found that this tradeoff was not mutually exclusive. In other words, cells that continue to cycle with a measurable increase in PPARG had some positive likelihood of differentiating later. Furthermore, we observed that PPARG levels can slowly keep rising during S/G2/M and, in rare cases even reach the estimated PPARG threshold for commitment to differentiation. Despite the observed tradeoff, our data demonstrates that cell division does not completely suppress the expression of the master regulator of adipogenesis. In differentiating cells, there is still an opportunity to enter the cell cycle. This is explained in part by the observed difference

in timescales. Whereas commitment to differentiation can take on average 26 hours from the birth of a cell, commitment to the next cell cycle may only take on average 6 hours from the birth of a cell.

In the third phase of the process, cells committed to differentiation and past the PPARG threshold become refractory to mitogenic signals and have a dramatically reduced probability of dividing in response to serum stimulation. This marks entry into the post-mitotic differentiated state and occurs before a cell fully becomes a mature fat cell. This regulation is due in part to the upregulation of the CDK inhibitor p21 by PPARG. Although we cannot say whether PPARG is a direct activator of the p21 promoter, it is clear from our data that upregulation of p21 by PPARG is both transcriptional and post-transcriptional.

An interesting observation from our data is that the PPARG-p21 relationship begins before cells commit to differentiation and may explain how cell cycle exit is often an early step in terminal differentiation. We observed reduced proliferation that was inversely correlated with the level of PPARG even in cells below the threshold. The correlation coefficient between PPARG and endpoints markers of adipocytes only turned positive after the PPARG threshold, suggesting that the PPARG threshold is when cells begin to become a canonical fat cell. This observation can be explained by the activation of positive feedback loops after the PPARG threshold that create the memory required to link early levels of PPARG to late expression of adipocyte genes. This may be a general feature of the transition into terminal differentiation since MyoD was also shown to inhibit the cell cycle separable from its ability to induce myogenic differentiation (Sorrentino et al., 1990).

In summary, our live cell data captures PPARG dynamics relative to cell cycle progression and allowed us to propose a dynamic three-phase model for the transition of proliferative precursors into post-mitotic differentiated cells. This model suggests that cells can control the balance between the precursor cell population and differentiated cell population by controlling the onset and duration of each of the three phases. Furthermore, under pathogenic conditions such as observed during cancer, our model suggests that continued cell cycle progression produces a tradeoff that reduces the likelihood of differentiation. However, this tradeoff is not completely mutually exclusive and can be modulated by effecting regulators of cell entry, and this fact may potentially be used for

therapeutic gain.

REFERENCES

Ahrends, R., Ota, A., Kovary, K.M., Kudo, T., Park, B.O., and Teruel, M.N. (2014). Controlling low rates of cell differentiation through noise and ultrahigh feedback. Science (80-.). *344*, 1384–1389.

Aragona, M., Dekoninck, S., Rulands, S., Lenglez, S., Mascré, G., Simons, B.D., and Blanpain, C. (2017). Defining stem cell dynamics and migration during wound healing in mouse skin epidermis. Nat. Commun. *8*, 14684.

Bahrami-Nejad, Z., Zhao, M.L., Tholen, S., Hunerdosse, D., Tkach, K.E., van Schie, S., Chung, M., and Teruel, M.N. (2018). A Transcriptional Circuit Filters Oscillating Circadian Hormonal Inputs to Regulate Fat Cell Differentiation. Cell Metab. *27*, 854-868.e8.

Baonza, A., and Freeman, M. (2005). Control of cell proliferation in the Drosophila eye by notch signaling. Dev. Cell *8*, 529–539.

Biteau, B., Hochmuth, C.E., and Jasper, H. (2011). Maintaining tissue homeostasis: dynamic control of somatic stem cell activity. Cell Stem Cell *9*, 402–411.

Blais, A., Tsikitis, M., Acosta-Alvear, D., Sharan, R., Kluger, Y., and Dynlacht, B.D. (2005). An initial blueprint for myogenic differentiation. Genes Dev. *19*, 553–569.

Buttitta, L.A., and Edgar, B.A. (2007). Mechanisms controlling cell cycle exit upon terminal differentiation. Curr. Opin. Cell Biol. *19*, 697–704.

Buttitta, L.A., Katzaroff, A.J., Perez, C.L., de la Cruz, A., and Edgar, B.A. (2007). A Double-Assurance Mechanism Controls Cell Cycle Exit upon Terminal Differentiation in Drosophila. Dev. Cell *12*, 631–643.

Cappell, S.D., Chung, M., Jaimovich, A., Spencer, S.L., and Meyer, T. (2016). Irreversible APCCdh1 Inactivation Underlies the Point of No Return for Cell-Cycle Entry. Cell *166*, 167–180.

Clayton, E., Doupé, D.P., Klein, A.M., Winton, D.J., Simons, B.D., and Jones, P.H. (2007). A single type of progenitor cell maintains normal epidermis. Nature *446*, 185–189.

Farmer, S.R. (2006). Transcriptional control of adipocyte formation. Cell Metab. *4*, 263–273.

Fu, M., Rao, M., Bouras, T., Wang, C., Wu, K., Zhang, X., Li, Z., Yao, T.P., and Pestell, R.G. (2005). Cyclin D1 inhibits peroxisome proliferator-activated receptor γ-mediated adipogenesis through histone deacetylase recruitment. J. Biol. Chem. *280*, 16934–16941.

Ghaben, A.L., and Scherer, P.E. (2019). Adipogenesis and metabolic health. Nat. Rev. Mol. Cell Biol. *20*, 242–258.

Guo, K., Wang, J., Andrés, V., Smith, R.C., and Walsh, K. (1995). MyoD-induced expression of p21 inhibits cyclin-dependent kinase activity upon myocyte terminal differentiation. Mol. Cell. Biol. *15*, 3823–3829.

Halevy, O., Novitch, B.G., Spicer, D.B., Skapek, S.X., Rhee, J., Hannon, G.J., Beach, D., and Lassar, A.B. (1995). Correlation of terminal cell cycle arrest of skeletal muscle with induction of p21 by MyoD. Science *267*, 1018–1021.

Hanahan, D., and Weinberg, R.A. (2011). Hallmarks of Cancer: The Next Generation. Cell *144*, 646–674.

Harris, T.E., Albrecht, J.H., Nakanishi, M., and Darlington, G.J. (2001). CCAAT/Enhancer-binding Protein-alpha Cooperates with p21 to Inhibit Cyclin-dependent Kinase-2 Activity and Induces Growth Arrest Independent of DNA Binding. J. Biol. Chem. *276*, 29200–29209.

Hsu, Y.-C., Li, L., and Fuchs, E. (2014). Transit-amplifying cells orchestrate stem cell activity and tissue regeneration. Cell *157*, 935–949.

Insco, M.L., Leon, A., Tam, C.H., McKearin, D.M., and Fuller, M.T. (2009). Accumulation of a differentiation regulator specifies transit amplifying division number in an adult stem cell lineage. Proc. Natl. Acad. Sci. U. S. A. *106*, 22311–22316.

Jascur, T., Brickner, H., Salles-Passador, I., Barbier, V., El Khissiin, A., Smith, B., Fotedar, R., and Fotedar, A. (2005). Regulation of p21WAF1/CIP1 Stability by WISp39, a Hsp90 Binding TPR Protein. Mol. Cell *17*, 237–249.

Jeffery, E., Church, C.D., Holtrup, B., Colman, L., and Rodeheffer, M.S. (2015). Rapid depot-specific activation of adipocyte precursor cells at the onset of obesity. Nat. Cell Biol. *17*, 376–385.

Jones, P.H., Simons, B.D., and Watt, F.M. (2007). Sic Transit Gloria: Farewell to the Epidermal Transit Amplifying Cell? Cell Stem Cell *1*, 371–381.

Kipreos, E.T., and van den Heuvel, S. (2019). Developmental Control of the Cell Cycle: Insights from Caenorhabditis elegans. Genetics *211*, 797–829.

Naaz, A., Holsberger, D.R., Iwamoto, G.A., Nelson, A., Kiyokawa, H., and Cooke, P.S. (2004). Loss of cyclin-dependent kinase inhibitors produces adipocyte hyperplasia and obesity. FASEB J. *15*, 1–15.

Park, B.O., Ahrends, R., and Teruel, M.N. (2012). Consecutive positive feedback loops create a bistable switch that controls preadipocyte-to-adipocyte conversion. Cell Rep. *2*, 976–990.
Parker, S., Eichele, G., Zhang, P., Rawls, A., Sands, A., Bradley, A., Olson, E., Harper, J., Elledge, S., Rawls, A., et al. (2006). p53-independent expression of p21Cip1 in muscle and other terminally differentiating cells. Science *267*, 1024–1027.
Ruijtenberg, S., and van den Heuvel, S. (2016). Coordinating cell proliferation and differentiation: Antagonism between cell cycle regulators and cell type-specific gene expression. Cell Cycle *15*, 196–212.
Ruijtenberg, S., van den Heuvel, S., and Van Den Heuvel, S. (2015). G1/S Inhibitors and the SWI/SNF Complex Control Cell-Cycle Exit during Muscle Differentiation. Cell *162*, 300–313.
Sakaue-Sawano, A., Kurokawa, H., Morimura, T., Hanyu, A., Hama, H., Osawa, H., Kashiwagi, S., Fukami, K., Miyata, T., Miyoshi, H., et al. (2008). Visualizing spatiotemporal dynamics of multicellular cell-cycle progression. Cell *132*, 487–498.
Sorrentino, V., Pepperkok, R., Davis, R.L., Ansorge, W., and Philipson, L. (1990). Cell proliferation inhibited by Myo01 independently of myogenic differentiation. Nature *345*, 813–815.
Spencer, S.L., Cappell, S.D., Tsai, F.C., Overton, K.W., Wang, C.L., and Meyer, T. (2013). The proliferation-quiescence decision is controlled by a bifurcation in CDK2 activity at mitotic exit. Cell *155*, 369–383.
Umek, R.M., Friedman, A.D., and McKnight, S.L. (1991). CCAAT-enhancer binding protein: a component of a differentiation switch. Science *251*, 288–292.
Wolins, N.E., Quaynor, B.K., Skinner, J.R., Tzekov, A., Park, C., Choi, K., and Bickel, P.E. (2006). OP9 mouse stromal cells rapidly differentiate into adipocytes: characterization of a useful new model of adipogenesis. J. Lipid Res. *47*, 450–460.
Zalc, A., Hayashi, S., Auradé, F., Bröhl, D., Chang, T., Mademtzoglou, D., Mourikis, P., Yao, Z., Cao, Y., Birchmeier, C., et al. (2014). Antagonistic regulation of p57 kip2 by Hes/Hey downstream of Notch signaling and muscle regulatory factors regulates skeletal muscle growth arrest. Development *141*, 2780–2790.

AUTHOR CONTRIBUTIONS

M.L.Z. and M.N.T. conceived experiments. M.L.Z., K.K., A.R., and Z.B. performed experiments and analyzed data. M.L.Z. and B.T. wrote the image analysis scripts. M.L.Z. and M.N.T wrote the paper with input from all authors.

ACKNOWLEDGEMENTS

This work was supported by National Institutes of Health RO1-DK101743, RO1-DK106241, P50-GM107615, a Stanford BioX Seed Grant, and a Stanford Diabetes Research Center Seed Grant (to M.N.T.), NIH F32 Postdoctoral Fellowship 5F32DK114981-02 (to B.T.), and T32-NIH T2HG00044 and NIH F31 Predoctoral Fellowship 1F31DK112570-01A1 (to M.L.Z.). The authors would like to thank Tobias Meyer, Takamasa Kudo, Antoine Zalc (Stanford) and members of Teruel lab for helpful discussions and critical reading of the manuscript.

FIGURE LEGENDS

Figure 1. Measurement of the precise time when cells irreversibly commit to differentiate based on live single-cell analysis of the expression level of PPARG

(A) (Top) Images of cells expressing endogenous citrine-PPARG were differentiated with the standard DMI protocol. (Bottom) Plot showing time course measurements of citrine-PPARG from two single cells – one that differentiated (blue) and one that remained undifferentiated (orange) over 4 days of imaging.

(B) Results of a typical differentiation experiment in which thousands of single cells were stimulated to differentiate. Traces are color coded based on whether they are differentiated cells (blue) or undifferentiated cells (orange) as assessed by PPARG levels.

(C) The scatter plot was generated from the experiment shown in Figure 1B and shows the PPARG levels from the 48-hour (x-axis) and 96-hour (y-axis) timepoints for each individual cell. Cells are color coded by differentiation status at the end of the experiment where blue represents differentiated cells and orange represents undifferentiated cells.

(D) Cells expressing endogenous citrine-PPARG were differentiated with the standard DMI protocol, and immunofluorescence was conducted at the end of the experiment for various markers of mature adipocytes. Endpoint citrine-PPARG (x-axis) is plotted against the various markers for differentiated fat cells (y-axis). Color gradient represents cell density. More than 4000 cells were used to create each scatter plot.

(E) This plot uses the data from Figure 1B. The single cell timecourses were split into equal width bins by their PPARG values at 0 (Start), 24, 48, and 72 hours. The bins ranged from 100-1900 with a bin width of 100. For each bin, the fraction of cells that were differentiated at the end of the experiment was calculated by dividing the number of cells that crossed the PPARG threshold by the total number of cells in the bin. The final empirical curves are estimates of the probability of differentiation for a given intensity level of PPARG. The dotted line represents the trough in between the bimodal PPARG histogram at the end of the experiment, and this point was used to determine whether a cell is differentiated.

(F) Differentiating cells were computationally aligned by the time point when PPARG threshold was crossed. Grey bold line represents the median trace, dark grey shaded region represents the 95th C.I., and the light grey shaded region represents the 5th-95th percentile trace. Overlaid are 5 representative individual single cell traces.

(G) PPARG time traces from differentiated cells in Figure 2D were computationally aligned by the PPARG threshold, with the zero timepoint representing the threshold crossing point. The blue line in each plot shows the mean PPARG value after alignment (n>1000 cells for each panel). Then for each aligned time point, the Pearson correlation coefficient between the aligned PPARG values and the endpoint immunofluorescence values for the various adipocyte markers was calculated and reported (orange line). As a comparison PPARG values for the Glut4 panel were aligned to a randomized PPARG threshold crossing point. The randomized crossing point was generated by taking the vector of measured threshold points for each cell and then scrambling the vector so that each threshold point is matched with different cell. Note that mean PPARG values and the correlation coefficient do not recapitulate key features present in the actual alignment.

Figure 2: Development of a system to measure timecourses of proliferation and terminal cell

differentiation dynamics simultaneously in thousands of individual cells.

(A) Cells stably expressing H2B-mTurqoise and geminin-degron-mCherry were imaged throughout a cell cycle. Bottom plot shows geminin accumulation in a representative single cell entering the cell cycle. Anaphase is shown by both a split in the H2B-mTurquoise signal (top images) and by a sharp drop in geminin signal (bottom timecourse).

(B) Dual reporter cells allow simultaneous measurement of differentiation state using PPARG levels (left plot) and cell cycle state using the geminin-degron sensor (right plot) in thousands of single cells. Dual reporter cells were stimulated to differentiate with DMI and observed continuously by microscopy for 4 days. The timepoints at which mitosis occurred were determined by using the split in H2B signal and are marked by the black open circles.

(C) Comparison of the number of observed mitotic events that occurred throughout the experiment from Figure 2B in cells that were differentiated at the end of the 4-day experiment versus cells that remained undifferentiated.

(D) Comparison of the duration of G1-phase, S/G2/M-phases, and total cell cycle duration (intermitotic time) for cells in the Figure 2B experiment that were differentiated at the end of the 4-day experiment versus cells that remained undifferentiated.

(E) Dual reporter cells were differentiated with the standard DMI protocol. Citrine-PPARG traces representing differentiation outcome (right) and mcherry-geminin traces representing cell cycle progression (left) are colored based on differentiation outcome. Blue traces mark cells that differentiated by day 4, and orange traces mark cells that remained undifferentiated throughout the experiment. The yellow dot in each plot marks the time at which that cell reached the PPARG threshold and irreversibly committed to the differentiated state.

Figure 3: Cells preferentially differentiate out of an extended G1 phase.

(A) A CDK2 sensor (orange trace) was added to the PPARG/geminin-degron dual reporter cells to create triple reporter cells. Triple reporter cells were differentiated using the standard DMI protocol, and a single representative trace is shown (left). The yellow dot represents the time when the cell reached the PPARG threshold and irreversibly committed to the differentiated state. The scatter plot (right) shows the CDK2 activity versus PPARG level in each single cell at every time point. The blue dashed line represents the PPARG threshold.

(B) Histogram of the difference between the time when the PPARG threshold is crossed and when mitosis last occurred for each cell. The PPARG threshold is reached on average ~14 hours after the last mitosis is completed. Negative values indicate cells that reach the PPARG threshold before the last mitosis is completed.

(C) In cells that underwent 2 or 3 observed mitoses before differentiating, we compared the time it takes to commit to the next cell cycle versus the time it takes it commit to differentiation. We used the second to last mitosis for each cell as the starting reference time. We then measured how long it took to upregulate geminin versus the how long it took to reach the PPARG threshold. n>2000 cells were used to make this comparison, and both values are measured for the same individual cell.

(D) Dual reporter preadipocyte cells from the time course experiment described in (A) were categorized into 9 bins based on the last mitosis time. (left) Each bin's last geminin trace peak is plotted to illustrate when the last mitosis occurred. (right) Each point on this plot represents the fraction of cells in each bin that differentiated versus the time spent in G1 before the differentiation commitment point is reached.

(E) Histograms comparing the duration of G1-phase, S/G2/M-phases, and total cell cycle duration (intermitotic time) for cells in the Figure 2B experiment that were differentiated at the end of the 4-day experiment (high PPARG) versus cells that remained undifferentiated (low PPARG).

Figure 4: The CDK inhibitor p21 and cyclin D, which both regulate the length of G1 phase, antagonistically regulate the number of differentiated cells.

(A) Dual reporter cells were transfected with siRNA against p21 or nontargeting siRNA and stimulated with the standard DMI differentiation protocol. Differentiation was assessed by counting cells that reached the PPARG threshold value at each time point and is represented by the fraction of differentiated cells over time. The percent of cells in the S/G2/M phases at each time point is calculated by counting the cells that showed expression of the geminin reporter during the 4-day differentiation timecourse divided by the total number of cells in the. The histogram shows the duration of the G1-phase for each of the individual siNeg (purple) versus sip21 (light blue) versus all (siNeg + sip21)(dark blue) cells.

(B) Dual reporter cells were stably infected with a construct constitutively expressing DHFR-p21-mCherry fusion protein. The cells were then differentiated with the standard DMI protocol in the presence of 10 µM TMP or DMSO. Differentiation and cell cycle status were assessed in the same manner as Figure 4A.

(C) Dual reporter cells were reverse transfected with siRNA targeting cyclin D1, cyclinD2/cyclinD3, or nontargeting siRNA (siControl). Differentiation and cell cycle status were determined in the same manner as in Figure 4A.

(D) To determine the effect of cyclin D knockdown on PPARG expression independent of cell cycle variation, cells with similar cell cycle properties were computationally selected for analysis of PPARG levels. Most cells transfected with siRNA targeting cyclin D proteins exhibited only 1 cell division. Therefore, the selection criteria used was for cells that went through one division in the first day of the experiment. The selection criteria were applied equally to all knockdown conditions. Median PPARG levels, along with the shaded 25th-75th percentile bounds (interquartile range, IQR), after selection are reported (left) and geminin degron levels are similarly reported (right).

(E) Dual reporter cells were differentiated using the standard DMI protocol but modified with reduced FBS media or the presence of a MEK inhibitor**.** Differentiation and cell cycle status were determined in the same manner as in Figure 4A.

(F) Schematic describing the pathway leading to commitment to the cell cycle.

Figure 5. PPARG controls cell cycle activity in part by upregulating p21 expression.

(A) Dual reporter cells were transfected with siRNA targeting PPARG and then stimulated to differentiate with the standard DMI protocol. Differentiation and cell cycle progression is reported as the fraction of cells past the PPARG threshold or the fraction of cells in S/G2/M phases as assessed by the presence of geminin signal for each time point, respectively.

(B) Wildtype OP9 cells were transfected with siRNA targeting PPARG or nontargeting siRNA and then stimulated to differentiate with the standard DMI protocol. Transcriptome samples were then collected daily for 6 days and subjected to RNA-seq analysis. All canonical CDK inhibitors were examined for their mRNA expression profiles over the course of differentiation for both siRNA

knockdown conditions. Each time point was collected in triplicates and data reported as mean transcripts per million (TPM) ± 1 standard deviation.

(C) Dual reporter cells were transfected with siRNA targeting p21, p18, or nontargeting siRNA and stimulated with the standard DMI protocol. The number of mitotic events per cell is reported in the normalized histograms.

(D) FKBPL expression under nontargeting or PPARG knockdown conditions obtained from the RNA-seq experiment in Figure 5B. Data reported as mean TPM ± 1 standard deviation.

(E) Wildtype OP9 cells were transfected with siRNA targeting FKBPL or nontargeting siRNA and stimulated to differentiate with the standard DMI cocktail for 48 hours. Stability of p21 and PPARG were assessed in the same cell by addition of 30 µM cycloheximide. Experiment done in triplicate and data plotted as mean ± 1 standard deviation.

(F) Wildtype OP9 cells were stimulated to differentiate by direct activation of PPARG with the small molecule agonist, rosiglitazone. Samples were fixed by PFA in 24-hour intervals for 5 days, and then immunofluorescence staining of PPARG and p21 was measured in the same cell. Data plotted as mean (line) along with the values for each of the three replicates (points). Red represents cells considered to be above the PPARG threshold, and blue represents cells considered to be below the PPARG threshold at a given timepoint. The PPARG threshold is assessed at day 5 and then the same value used for all preceding days.

(G) Dual reporter cells were stimulated to differentiate with the standard DMI protocol and PPARG levels in differentiated (red) and undifferentiated (blue) cells were computationally aligned by entry into the last observed S phase. Plotted are population medians and the shaded region represents the IQR. Bottom plots show the aligned geminin signal in each cell population.

(H) The fraction of all cells in S/G2/M phases (dashed) or past the PPARG threshold (solid) from (A) were plotted over time (left). The blue line (right) represents the fraction of cells in S/G2/M at every timepoint, from 0-72 hours, that ultimately differentiate at the end of the experiment. This is done by first selecting for all cells that are currently in S/G2/M at every time point, then calculating the fraction of cells in that group that are considered differentiated at the end of the experiment. In red are the fraction of all cells at each time point that are committed to cell division (in S/G2/M, dotted red line) or committed to differentiation (solid red line).

(I) Schematic connecting PPARG signaling with the regulation of cell cycle commitment through the regulation of p21 expression.

Figure 6. PPARG induced p21 expression brings cells into a post-mitotic state associated with differentiation.

(A) Dual reporter cells were stimulated to differentiate with the standard DMI protocol. The relationship between PPARG levels and cell cycle progression in response to media replacement at 48 hours was measured by imaging citrine-PPARG and geminin levels. Cells were separated into bins based on the PPARG levels before the media is changed from DMI to media with just insulin and growth factors around the 48-hour timepoint. The corresponding mean PPARG and geminin-degron signals are plotted for each bin. The bins are equally spaced.

(B) Cells in Figure 6A were separated into 11 equally spaced bins from based on their PPARG levels prior to the media switch. Then the fraction of cells in each bin that divide at least once after the media switch, as assessed by the split of H2B fluorescence after anaphase of mitosis, is plotted. The dotted line marks the value estimated to be the PPARG threshold.

(C) Dual reporter cells were fixed at the end of a differentiation experiment and immunofluorescence was performed for p21. Cells were placed into equally spaced bins according to their final citrine-PPARG levels and the average p21 intensity was plotted for each bin. The dotted line marks the value estimated to be the PPARG threshold.

(D-E) Dual reporter cells were stimulated to differentiate with the standard DMI protocol. Then siRNA targeting PPARG, CEBPA, p21, or nontargeting siRNA was transfected into the dual reporter cells at the 48-hour timepoint. For each siRNA condition, differentiation and cell cycle progression was assessed in a manner previously described. Knockdown efficacy was assessed by endpoint staining of p21 and CEBPA while PPARG knockdown efficacy was assessed by miCtrine-PPARG fluorescence (Figure S5).

(F) Images showing that when p21 is knocked down in differentiated fat cells, defects such as multi-nucleated cells are apparent (red arrows). Dual reporter OP9 cells were induced to differentiate using a 4-day DMI stimulus protocol and then transfected with siRNA targeting p21 or non-targeting (control) siRNA. Cells were imaged 2 days after siRNA transfection. To assess nuclear structure, the H2B-mTurquoise(CFP) expression is shown.

(G) The same analysis described in Figure 6A was performed on the knockdown experiment in Figure 6D for the p21 knockdown or nontargeting siRNA conditions.

(H) Wildtype OP9 cells were stimulated to differentiate with the direct PPARG agonist, rosiglitazone. Cells were fixed with PFA at day 0, day 1, and day 3 of differentiation and immunofluorescence staining was performed for PPARG, p21, and cyclin D1 expression in the same cell. Scatter plots for the cyclin D1 versus p21 levels are color coded based on PPARG level (left) representing differentiated or undifferentiated cells. Histograms at the right show the degree of differentiation at each day with the dotted line demarcating the separation between differentiated and undifferentiated cells.

Figure 7. Terminal cell differentiation and cell cycle exit is precisely timed by coincident induction of the CDK-inhibitor p21

(A) Timecourse data from Figure 5I demonstrate how the post-mitotic state is achieved as a cell progresses through terminal differentiation.

(B) Schematic of the three stages. During the intermediate phase, cells can probabilistically exit into a differentiated or proliferating state. This phase defines how many differentiated cells are generated on average from a precursor cell. In this phase, p21 and/or p27 are only partially engaged, and cell density might be higher due to the initial cell expansion phase.

EXTENDED FIGURE LEGENDS

Figure S1. In comparison to using PPARG abundance to predict final differentiated state (Figure 1E), both the integral and derivative values of PPARG served as poorer predictors of the final differentiated state.

Figure S2. Analysis of the PPARG derivative around the PPARG threshold point shows that the change occurs fast relative to the four-day time course, with a large increase in PPARG occurring in a 3-hour window around the threshold point.

Figure S3. The subconfluent plating conditions used in this study yielded 20-50% differentiated cells after 4 days of differentiation compared to ~80% differentiation rate under more confluent conditions.

Figure S4. Dilution through cell division does not significantly affect PPARG dynamics in differentiated cells.

(A) PPARG dynamics in differentiated cells were compared between cells that divided two or three times in the span of the experiment.

(B) The tradeoff between continued proliferation and differentiation exists even in cells that have been selected for undergoing exactly two divisions throughout the live-cell experiment.

Figure S5. Validation of the siRNA knockdown efficiency in Figure 6.

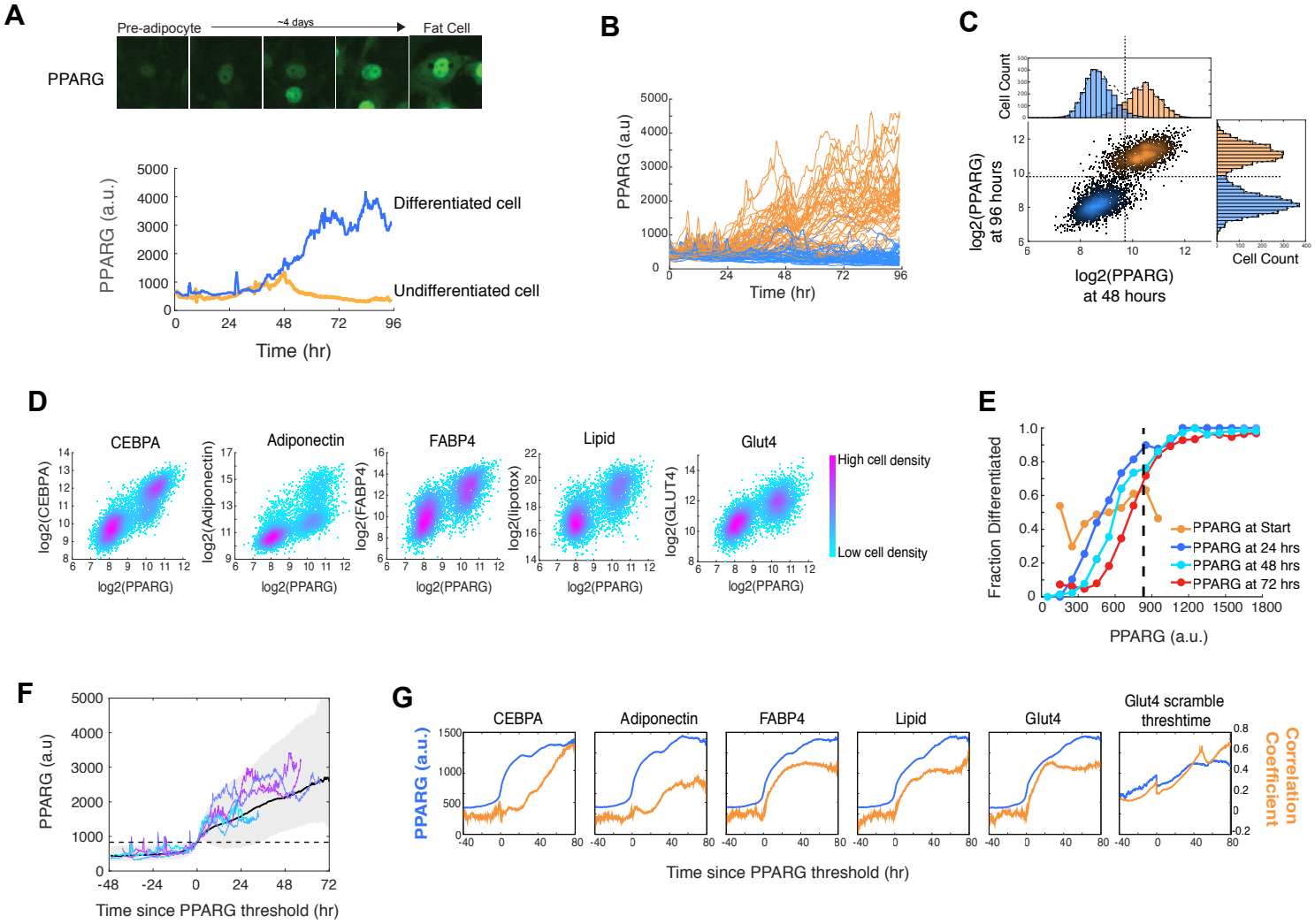

Figure 1. Measurement of the precise time when cells irreversibly commit to differentiate based on live single-cell analysis of the expression level of PPARG

(A) (Top) Images of cells expressing endogenous citrine-PPARG were differentiated with the standard DMI protocol. (Bottom) Plot showing time course measurements of citrine-PPARG from two single cells – one that differentiated (blue) and one that remained undifferentiated (orange) over 4 days of imaging.

(B) Results of a typical differentiation experiment in which thousands of single cells were stimulated to differentiate. Traces are color coded based on whether they are differentiated cells (blue) or undifferentiated cells (orange) as assessed by PPARG levels.

(C) The scatter plot was generated from the experiment shown in Figure 1B and shows the PPARG levels from the 48-hour (x-axis) and 96-hour (y-axis) timepoints for each individual cell. Cells are color coded by differentiation status at the end of the experiment where blue represents differentiated cells and orange represents undifferentiated cells.

(D) Cells expressing endogenous citrine-PPARG were differentiated with the standard DMI protocol, and immunofluorescence was conducted at the end of the experiment for various markers of mature adipocytes. Endpoint citrine-PPARG (x-axis) is plotted against the various markers for differentiated fat cells (y-axis). Color gradient represents cell density. More than 4000 cells were used to create each scatter plot.

(E) This plot uses the data from Figure 1B. The single cell timecourses were split into equal width bins by their PPARG values at 0 (Start), 24, 48, and 72 hours. The bins ranged from 100-1900 with a bin width of 100. For each bin, the fraction of cells that were differentiated at the end of the experiment was calculated by dividing the number of cells that crossed the PPARG threshold by the total number of cells in the bin. The final empirical curves are estimates of the probability of differentiation for a given intensity level of PPARG. The dotted line represents the trough in between the bimodal PPARG histogram at the end of the experiment, and this point was used to determine whether a cell is differentiated.

(F) Differentiating cells were computationally aligned by the time point when PPARG threshold was crossed. Grey bold line represents the median trace, dark grey shaded region represents the 95th C.I., and the light grey shaded region represents the 5th-95th percentile trace. Overlaid are 5 representative individual single cell traces.

(G) PPARG time traces from differentiated cells in Figure 2D were computationally aligned by the PPARG threshold, with the zero timepoint representing the threshold crossing point. The blue line in each plot shows the mean PPARG value after alignment (n > 1000 cells for each panel). Then for each aligned time point, the Pearson correlation coefficient between the aligned PPARG values and the endpoint immunofluorescence values for the various adipocyte markers was calculated and reported (orange line). As a comparison PPARG values for the Glut4 panel were aligned to a randomized PPARG threshold crossing point. The randomized crossing point was generated by taking the vector of measured threshold points for each cell and then scrambling the vector so that each threshold point is matched with different cell. Note that mean PPARG values and the correlation coefficient do not recapitulate key features present in the actual alignment.

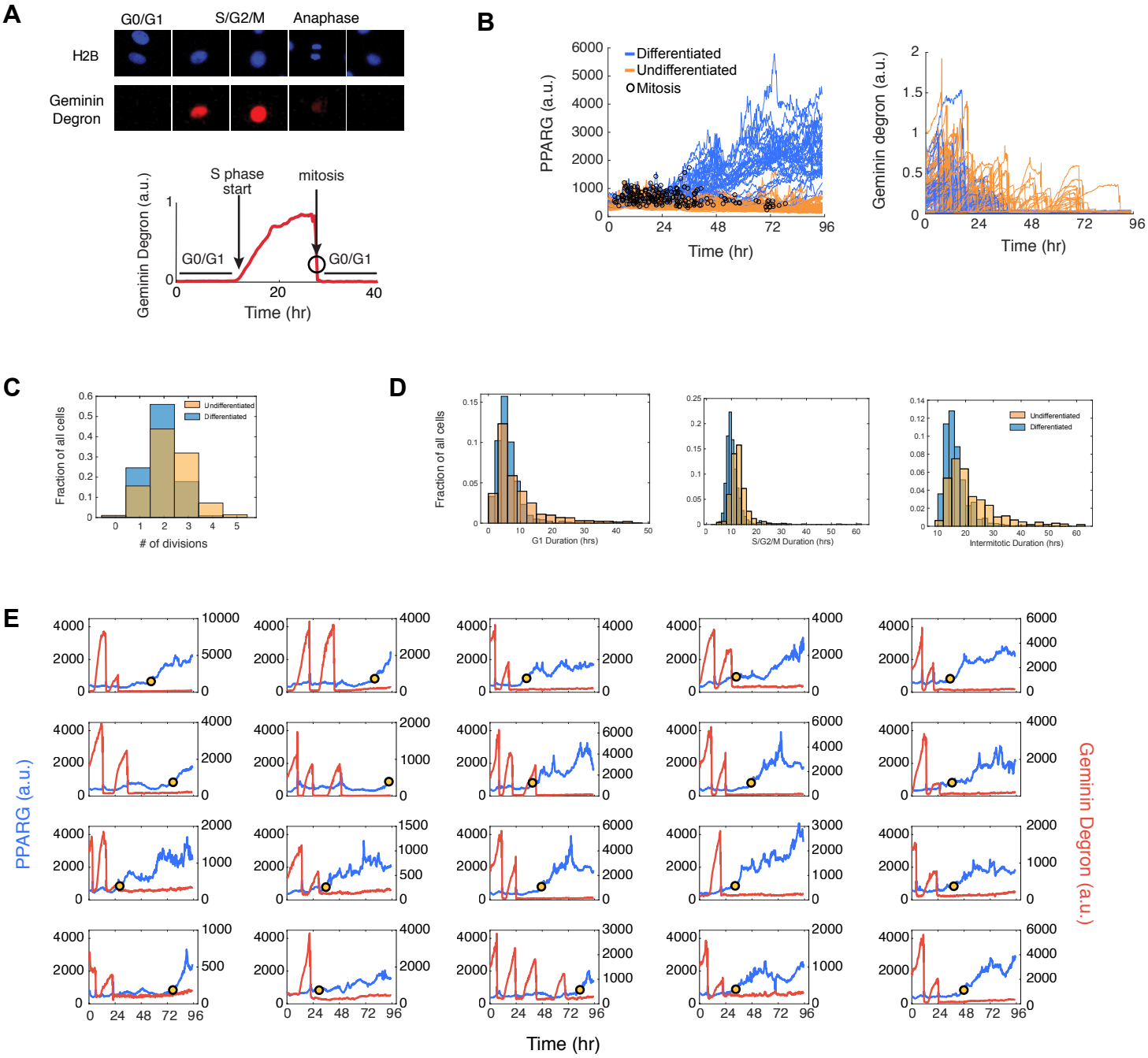

Figure 2: Development of a system to measure timecourses of proliferation and terminal cell differentiation dynamics simultaneously in thousands of individual cells.

(A) Cells stably expressing H2B-mTurqoise and geminin-degron-mCherry were imaged throughout a cell cycle. Bottom plot shows geminin accumulation in a representative single cell entering the cell cycle. Anaphase is shown by both a split in the H2B-mTurquoise signal (top images) and by a sharp drop in geminin signal (bottom timecourse).

(B) Dual reporter cells allow simultaneous measurement of differentiation state using PPARG levels (left plot) and cell cycle state using the geminin-degron sensor (right plot) in thousands of single cells. Dual reporter cells were stimulated to differentiate with DMI and observed continuously by microscopy for 4 days. The timepoints at which mitosis occurred were determined by using the split in H2B signal and are marked by the black open circles.

(C) Comparison of the number of observed mitotic events that occurred throughout the experiment from Figure 2B in cells that were differentiated at the end of the 4-day experiment versus cells that remained undifferentiated.

(D) Comparison of the duration of G1-phase, S/G2/M-phases, and total cell cycle duration (intermitotic time) for cells in the Figure 2B experiment that were differentiated at the end of the 4-day experiment versus cells that remained undifferentiated.

(E) Dual reporter cells were differentiated with the standard DMI protocol. Citrine-PPARG traces representing differentiation outcome (right) and mcherry-geminin traces representing cell cycle progression (left) are colored based on differentiation outcome. Blue traces mark cells that differentiated by day 4, and orange traces mark cells that remained undifferentiated throughout the experiment. The yellow dot in each plot marks the time at which that cell reached the PPARG threshold and irreversibly committed to the differentiated state.

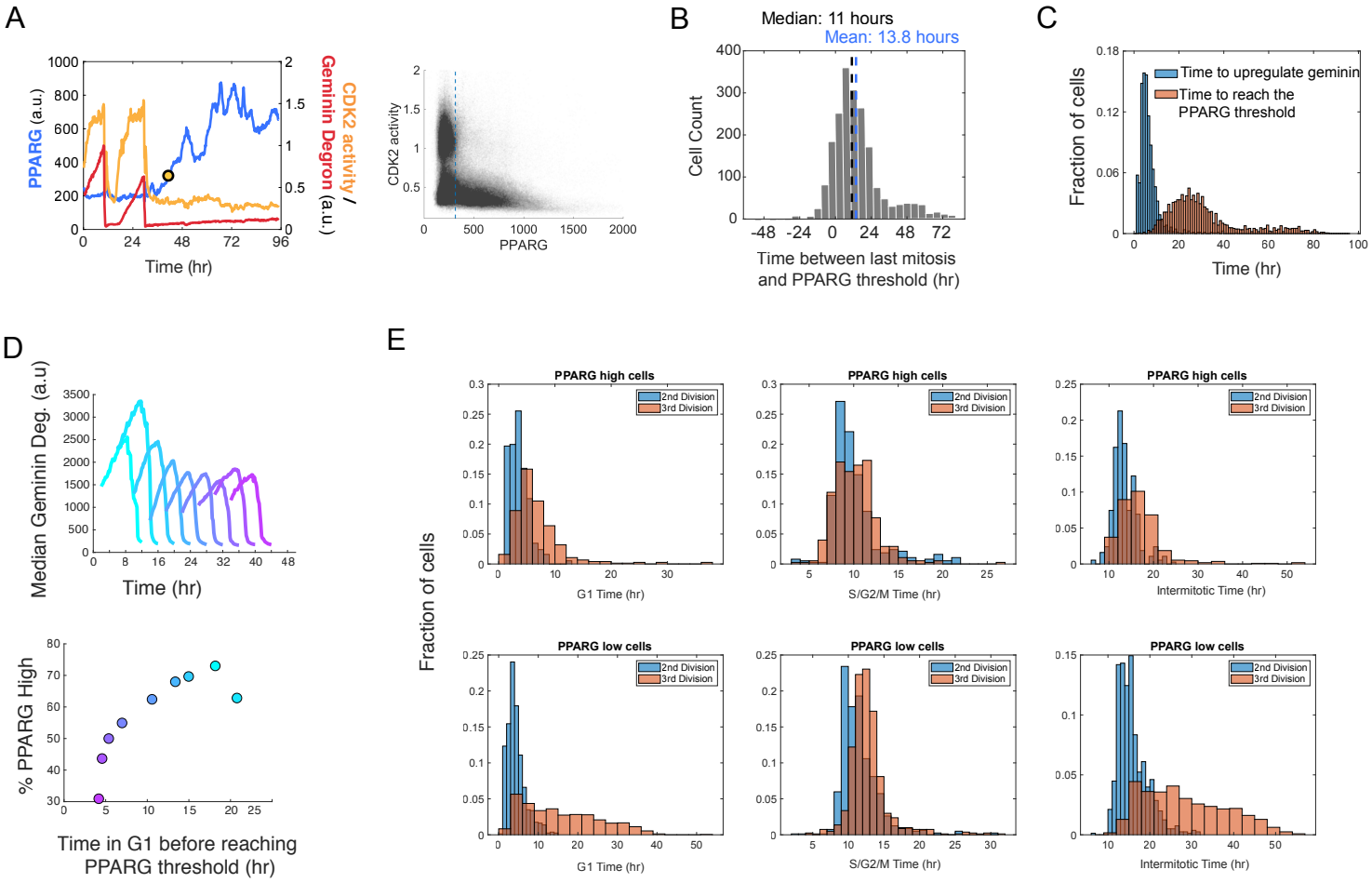

Figure 3: Cells preferentially commit to differentiate out of an extended G1 phase.
(A) A CDK2 sensor (orange trace) was added to the PPARG/geminin-degron dual reporter cells to create triple reporter cells. Triple reporter cells were differentiated using the standard DMI protocol, and a single representative trace is shown (left). The yellow dot represents the time when the cell reached the PPARG threshold and irreversibly committed to the differentiated state. The scatter plot (right) shows the CDK2 activity versus PPARG level in each single cell at every time point. The blue dashed line represents the PPARG threshold.
(B) Histogram of the difference between the time when the PPARG threshold is crossed and when mitosis last occurred for each cell. The PPARG threshold is reached on average ~14 hours after the last mitosis is completed. Negative values indicate cells that reach the PPARG threshold before the last mitosis is completed.
(C) In cells that underwent 2 or 3 observed mitoses before differentiating, we compared the time it takes to commit to the next cell cycle versus the time it takes it commit to differentiation. We used the second to last mitosis for each cell as the starting reference time. We then measured how long it took to upregulate geminin versus the how long it took to reach the PPARG threshold. n>2000 cells were used to make this comparison, and both values are measured for the same individual cell.
(D) Dual reporter preadipocyte cells from the time course experiment described in (A) were categorized into 9 bins based on the last mitosis time. (left) Each bin's last geminin trace peak is plotted to illustrate when the last mitosis occurred. (right) Each point on this plot represents the fraction of cells in each bin that differentiated versus the time spent in G1 before the differentiation commitment point is reached.
(E) Histograms comparing the duration of G1-phase, S/G2/M-phases, and total cell cycle duration (intermitotic time) for cells in the Figure 2B experiment that were differentiated at the end of the 4-day experiment (high PPARG) versus cells that remained undifferentiated (low PPARG).

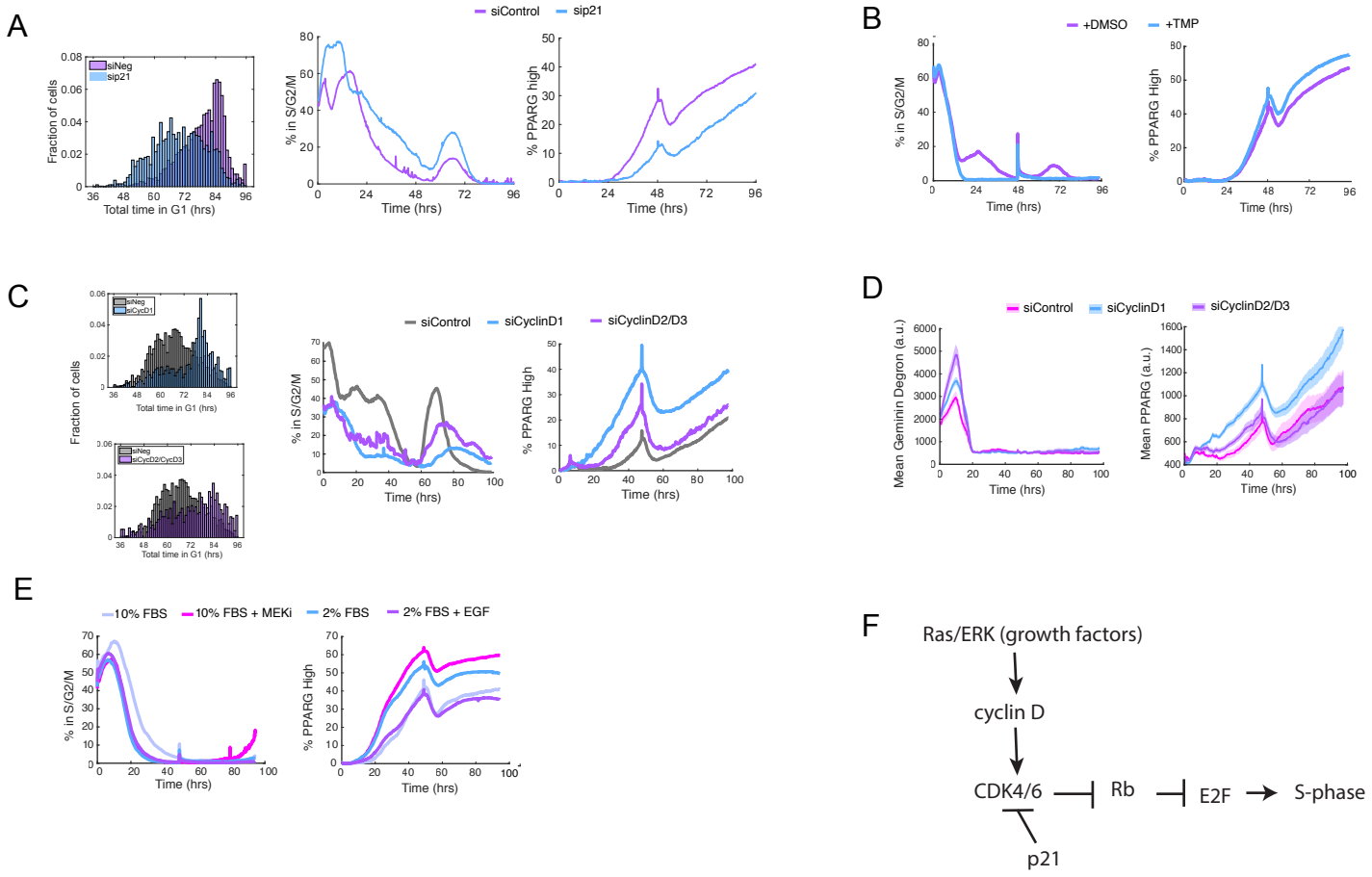

Figure 4: The CDK inhibitor p21 and cyclin D, which both regulate the length of G1 phase, antagonistically regulate the number of differentiated cells.

(A) Dual reporter cells were transfected with siRNA against p21 or nontargeting siRNA and stimulated with the standard DMI differentiation protocol. Differentiation was assessed by counting cells that reached the PPARG threshold value at each time point and is represented by the fraction of differentiated cells over time. The percent of cells in the S/G2/M phases at each time point is calculated by counting the cells that showed expression of the geminin reporter during the 4-day differentiation timecourse divided by the total number of cells in the. The histogram shows the duration of the G1-phase for each of the individual siNeg (purple) versus sip21 (light blue) versus all (siNeg and sip21)(dark blue) cells.

(B) Dual reporter cells were stably infected with a construct constitutively expressing DHFR-p21-mCherry fusion protein. The cells were then differentiated with the standard DMI protocol in the presence of 10 μM TMP or DMSO. Differentiation and cell cycle status wereassessed in the same manner as Figure 4A.

(C) Dual reporter cells were reverse transfected with siRNA targeting cyclin D1, cyclinD2/cyclinD3, or nontargeting siRNA (siControl). Differentiation and cell cycle status were determined in the same manner as in Figure 4A. The histogram shows the duration of the G1-phase for each of the individual siNeg (grey) versus siCyclinD (light blue or light purple) versus all (siNeg+siCyclin)(dark blue and dark purple) cells.

(D) To determine the effect of cyclin D knockdown on PPARG expression independent of cell cycle variation, cells with similar cell cycle properties were computationally selected for analysis of PPARG levels. Most cells transfected with siRNA targeting cyclin D proteins exhibited only 1 cell division. Therefore, the selection criteria used was for cells that went through one division in the first day of the experiment. The selection criteria were applied equally to all knockdown conditions. Median PPARG levels, along with the shaded 25th-75th percentile bounds (interquartile range, IQR), after selection are reported (left) and geminin degron levels are similarly reported (right).

(E) Dual reporter cells were differentiated using the standard DMI protocol but modified with reduced FBS media or the presence of a MEK inhibitor. Differentiation and cell cycle status were determined in the same manner as in Figure 4A.

(F) Schematic describing the pathway leading to commitment to the cell cycle.

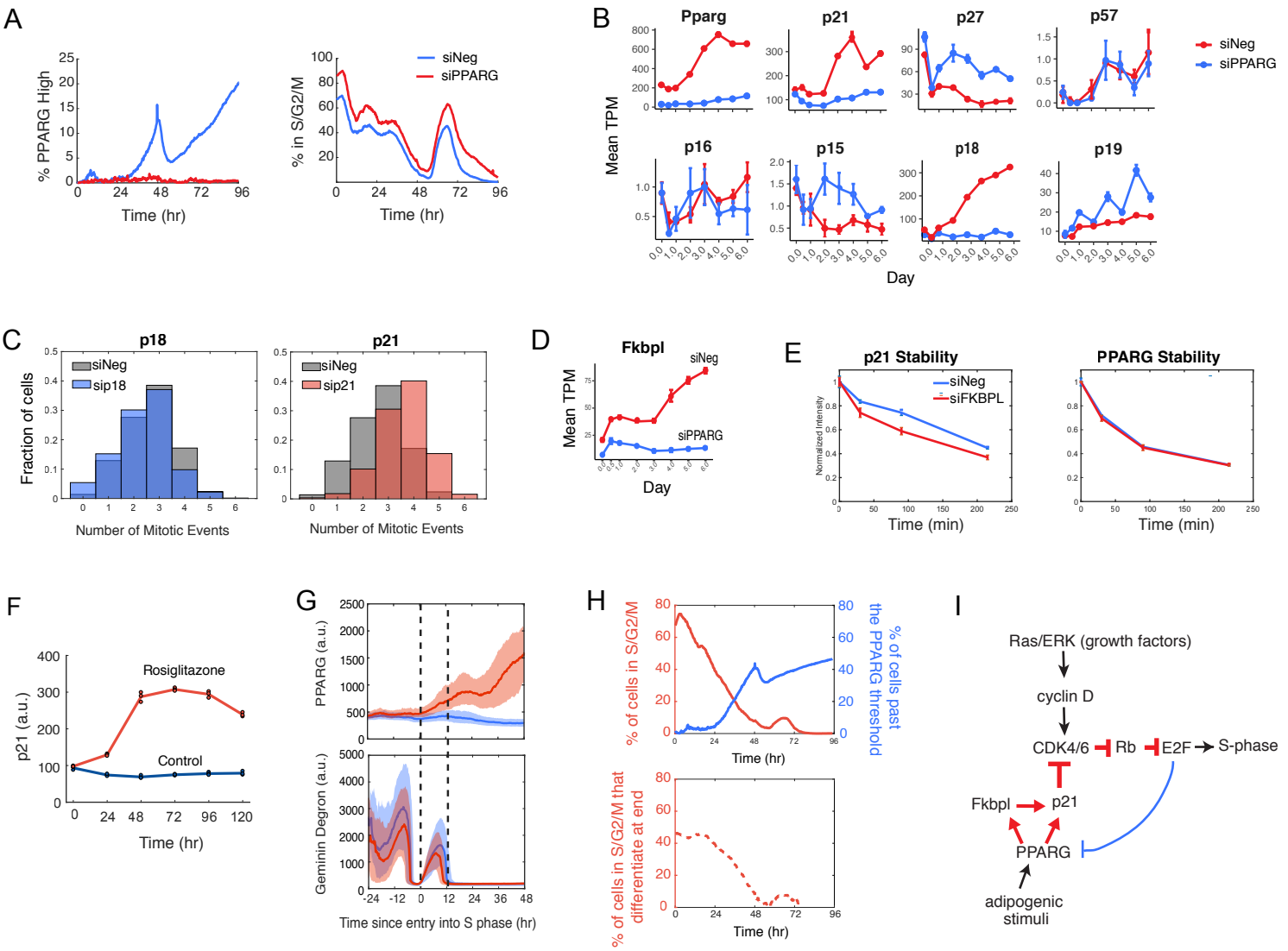

Figure 5. PPARG controls cell cycle activity in part by upregulating p21 expression.
(A) Dual reporter cells were transfected with siRNA targeting PPARG and then stimulated to differentiate with the standard DMI protocol. Differentiation and cell cycle progression is reported as the fraction of cells past the PPARG threshold or the fraction of cells in S/G2/M phases as assessed by the presence of geminin signal for each time point, respectively.
(B) Wildtype OP9 cells were transfected with siRNA targeting PPARG or nontargeting siRNA and then stimulated to differentiate with the standard DMI protocol. Transcriptome samples were then collected daily for 6 days and subjected to RNA-seq analysis. All canonical CDK inhibitors were examined for their mRNA expression profiles over the course of differentiation for both siRNA knockdown conditions. Each time point was collected in triplicates and data reported as mean transcripts per million (TPM) ± 1 standard deviation.
(C) Dual reporter cells were transfected with siRNA targeting p21, p18, or nontargeting siRNA and stimulated with the standard DMI protocol. The number of mitotic events per cell is reported in the normalized histograms.
(D) FKBPL expression under nontargeting or PPARG knockdown conditions obtained from the RNA-seq experiment in Figure 5B. Data reported as mean TPM ± 1 standard deviation.
(E) Wildtype OP9 cells were transfected with siRNA targeting FKBPL or nontargeting siRNA and stimulated to differentiate with the standard DMI cocktail for 48 hours. Stability of p21 and PPARG were assessed in the same cell by addition of 30 μM cycloheximide. Experiment done in triplicate and data plotted as mean ± 1 standard deviation.
(F) Wildtype OP9 cells were stimulated to differentiate by direct activation of PPARG with the small molecule agonist, rosiglitazone. Samples were fixed by PFA in 24-hour intervals for 5 days, and then immunofluorescence staining of PPARG and p21 was measured in the same cell. Data plotted as mean (line) along with the values for each of the three replicates (points). Red represents cells considered to be above the PPARG threshold, and blue represents cells considered to be below the PPARG threshold at a given timepoint. The PPARG threshold is assessed at day 5 and then the same value used for all preceding days.
(G) Dual reporter cells were stimulated to differentiate with the standard DMI protocol and PPARG levels in differentiated (red) and undifferentiated (blue) cells were computationally aligned by entry into the last observed S phase. Plotted are population medians and the shaded region represents the IQR. Bottom plots show the aligned geminin signal in each cell population.
(H) The fraction of all cells in S/G2/M phases (dashed) or past the PPARG threshold (solid) from (A) were plotted over time (left). The blue line (right) represents the fraction of cells in S/G2/M at every timepoint, from 0-72 hours, that ultimately differentiate at the end of the experiment. This is done by first selecting for all cells that are currently in S/G2/M at every time point, then calculating the fraction of cells in that group that are considered differentiated at the end of the experiment. In red are the fraction of all cells at each time point that are committed to cell division (in S/G2/M, dotted red line) or committed to differentiation (solid red line).
(I) Schematic connecting PPARG signaling with the regulation of cell cycle commitment through the regulation of p21 expression.

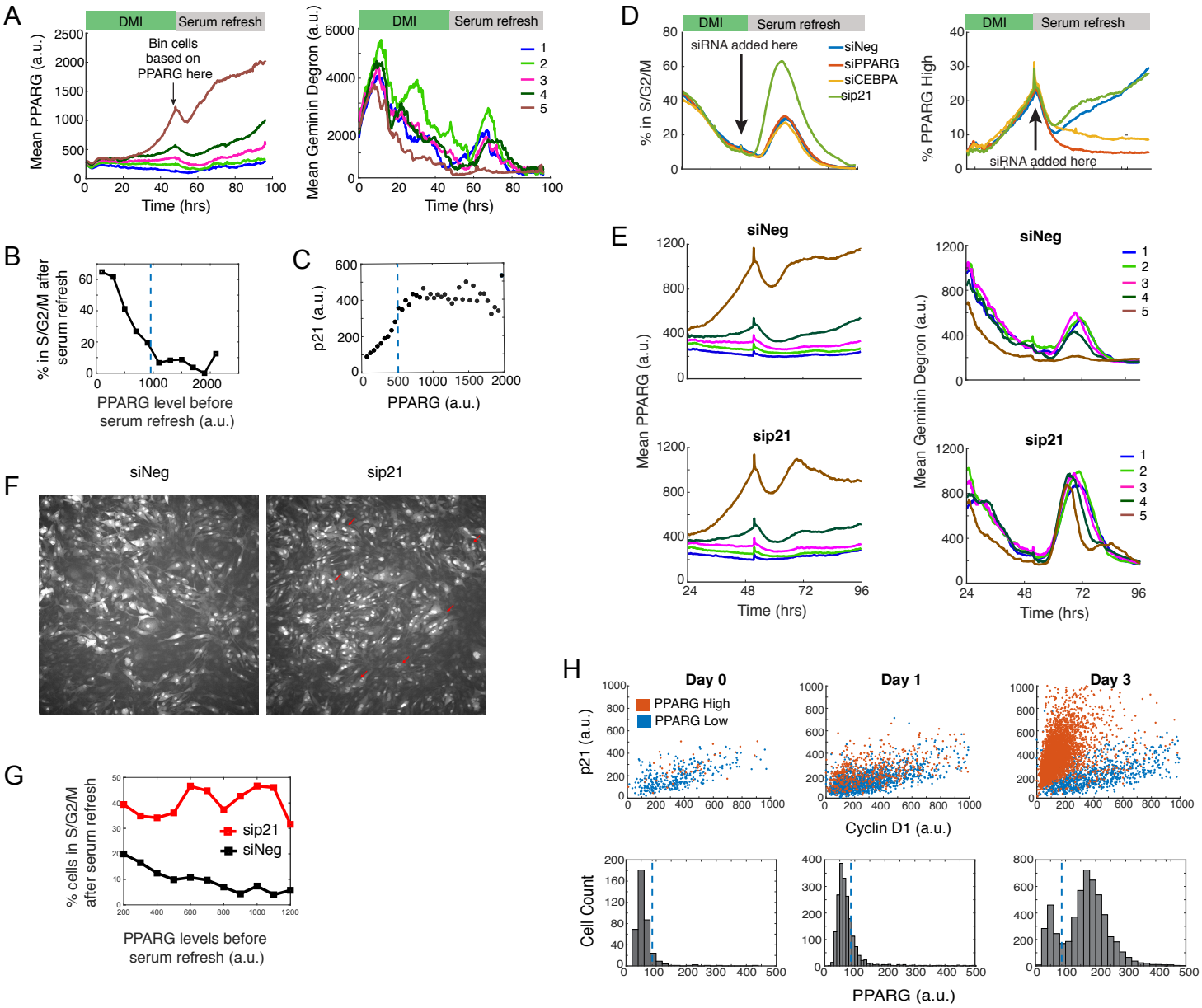

Figure 6. PPARG induced p21 expression brings cells into a post-mitotic state associated with differentiation.
(A) Dual reporter cells were stimulated to differentiate with the standard DMI protocol. The relationship between PPARG levels and cell cycle progression in response to media replacement at 48 hours was measured by imaging citrine-PPARG and geminin levels. Cells were separated into bins based on the PPARG levels before the media is changed from DMI to media with just insulin and growth factors around the 48-hour timepoint. The corresponding mean PPARG and geminin-degron signals are plotted for each bin. The bins are equally spaced.
(B) Cells in Figure 6A were separated into 11 equally spaced bins from based on their PPARG levels prior to the media switch. Then the fraction of cells in each bin that divide at least once after the media switch, as assessed by the split of H2B fluorescence after anaphase of mitosis, is plotted. The dotted line marks the value estimated to be the PPARG threshold.
(C) Dual reporter cells were fixed at the end of a differentiation experiment and immunofluorescence was performed for p21. Cells were placed into equally spaced bins according to their final citrine-PPARG levels and the average p21 intensity was plotted for each bin. The dotted line marks the value estimated to be the PPARG threshold.
(D-E) Dual reporter cells were stimulated to differentiate with the standard DMI protocol. Then siRNA targeting PPARG, CEBPA, p21, or nontargeting siRNA was transfected into the dual reporter cells at the 48-hour timepoint. For each siRNA condition, differentiation and cell cycle progression was assessed in a manner previously described. Knockdown efficacy was assessed by endpoint staining of p21 and CEBPA while PPARG knockdown efficacy was assessed by miCtrine-PPARG fluorescence (Figure S5).
(F) Images showing that when p21 is knocked down in differentiated fat cells, defects such as multi-nucleated cells are apparent (red arrows). Dual reporter OP9 cells were induced to differentiate using a 4-day DMI stimulus protocol and then transfected with siRNA targeting p21 or non-targeting (control) siRNA. Cells were imaged 2 days after siRNA transfection. To assess nuclear structure, the H2B-mTurquoise(CFP) expression is shown.
(G) The same analysis described in Figure 6A was performed on the knockdown experiment in Figure 6D for the p21 knockdown or nontargeting siRNA conditions.
(H) Wildtype OP9 cells were stimulated to differentiate with the direct PPARG agonist, rosiglitazone. Cells were fixed with PFA at day 0, day 1, and day 3 of differentiation and immunofluorescence staining was performed for PPARG, p21, and cyclin D1 expression in the same cell. Scatter plots for the cyclin D1 versus p21 levels are color coded based on PPARG level (left) representing differentiated or undifferentiated cells. Histograms at the right show the degree of differentiation at each day with the dotted line demarcating the separation between differentiated and undifferentiated cells.

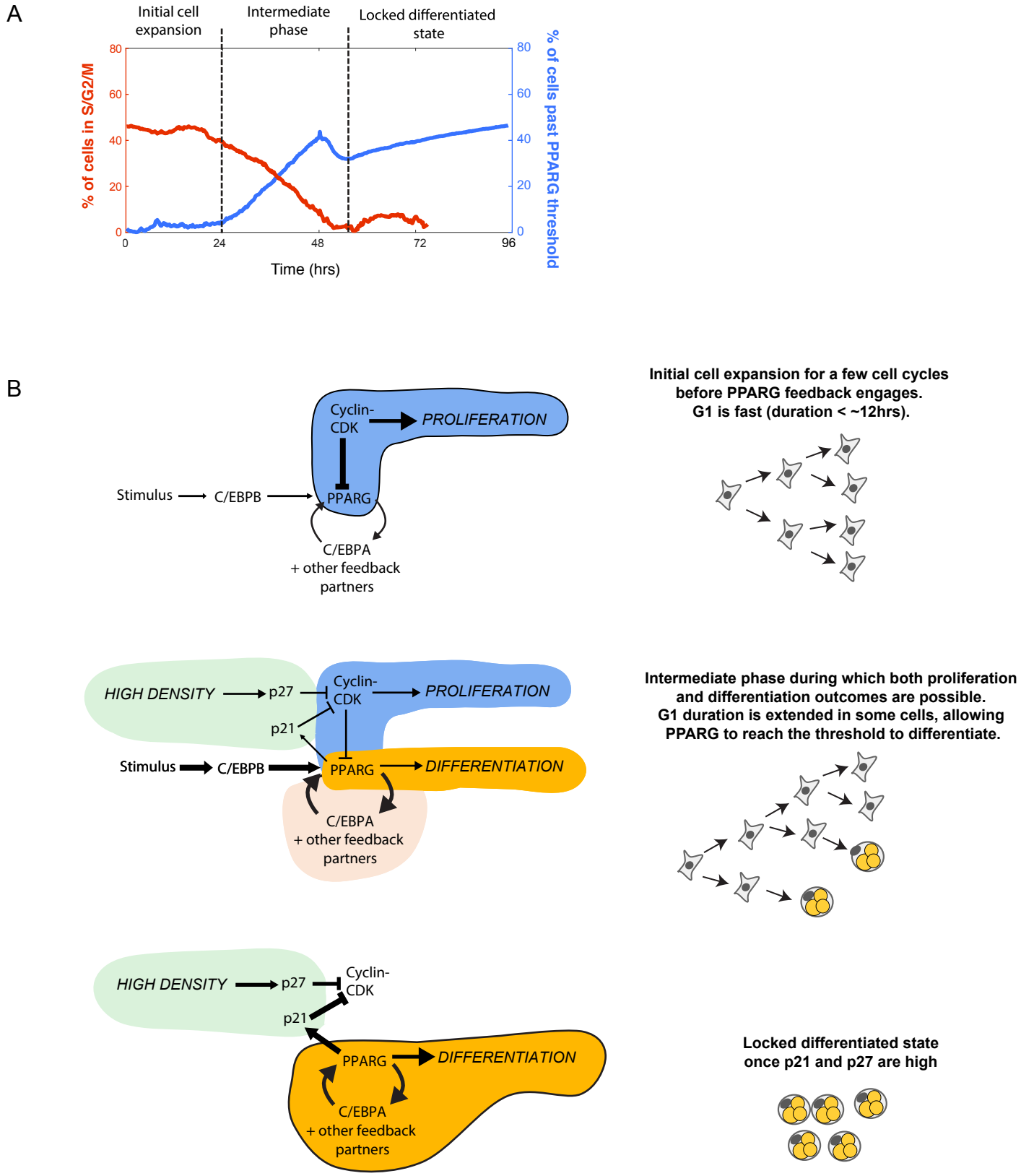

Figure 7. Terminal cell differentiation and cell cycle exit is precisely timed by coincident induction of the CDK-inhibitor p21
(A) Timecourse data from Figure 5I demonstrates how the post-mitotic state is achieved through as a cell progresses through terminal differentiation.
(B) Description of the three phases of terminal cell differentiation. During the intermediate phase, cells can probabilistically exit into a differentiated or proliferating state. This phase defines how many differentiated cells are generated on average from a precursor cell. In this phase, p21 and/or p27 are only partially engaged, and cell density might be higher due to the initial cell expansion phase.